Ann. Naturhist. Mus. Wien	100 A	13–38	Wien, Juli 1999

Textural studies of altered/metamorphosed tuffs and secondary REE-, Zr- and Y-minerals: scanning electron microscopic examinations

by J.H. OBENHOLZNER[1] & G. HEIKEN[2]

(With 16 text-figures)

Manuscript submitted on August 13th 1998,
the revised manuscript on October 21st 1998

Abstract

Lithified volcaniclastic rocks form significant strata in the sedimentological record, but alteration by diagenetic/metamorphic processes in many cases prevent characterization of eruption and emplacement histories. Indeed, lithification prevents adequate disaggregation and separation of pyroclasts from these tuffs. Volcanic ash shards, pumice fragments and magmatic minerals have been partially or totally replaced by secondary minerals, and have been cemented through diagenesis or metamorphism. The alteration/lithification processes can also provide the environment for rare mineral formation. Especially secondary REE-, Zr- and Y-bearing minerals are far more widespread than assumed.

In developing the SEM as a petrographic tool to unravel the multitude of textural features of altered and lithified volcanic ash, we discribe a technique of using digitized backscattered electron (BSE) images that enhance the pyroclast shapes or their relict textures in polished thin sections. Being able to observe the shard shapes and pumice fragments allow conclusions to be made about eruption mechanisms responsible for the tuff deposit. The reconstruction of chemical and physical properties of ancient tuffs eases comparison with more recent ashes.

Keywords: pyroclast relict texture, altered and lithified volcanic ash/tuff, SEM, secondary REE-, Zr-, Y-bearing minerals.

Zusammenfassung

Vulkanoklastische Gesteine stellen einen bedeutender Anteil an den Sedimenten dar. Alteration durch Diagenese oder Metamorphose verhindert in vielen Fällen eine Charakterisierung der Eruptions-, bzw. Ablagerungsgeschichte. In Folge der Lithifikation ist eine adequate Partikeltrennung oder Separation von Pyroklasten dieser Tuffe unmöglich. Vulkanische Glasscherben, Bimsfragmente und magmatische Minerale sind teilweise oder gänzlich ersetzt durch Sekundärminerale, und können durch Diagenese oder Metamorphose zementiert sein. Der Alterationsprozess kann auch das Environment für die Bildung von seltenen Mineralen darstellen. Speziell sekundäre SEE-, Zr- und Y-führende Minerale sind weiter verbreitet als angenommen.

Wir haben das Rasterelektronenmikroskop als Instrument eingesetzt, die Vielzahl von Gefügen lithifizierter Tuffe zu analysieren. Es wird eine Methode beschrieben, mittels rückgestreuter Elektronenbilder die

[1] Naturhistorisches Museum, Mineralogische Abteilung, Postfach 417, A-1014 Vienna, Austria (e-mail: mineralogie@nhm-wien.ac.at)

[2] EES-1, Geology/Geochemistry, Los Alamos National Laboratory, Los Alamos, NM 87545, USA.

Form von Pyroklasten, bzw. deren Reliktstrukturen im polierten Dünnschliff darzustellen. Die Form der Scherben und Bimsfragmente ermöglicht Rückschlüsse auf den Eruptionsmechanismus, der den Tuffablagerungen vorausgegangen ist. Eine Rekonstruktion der physikalischen und chemischen Eigenschaften lithifizierter Tuffe ermöglicht auch einen Vergleich mit gut studierten vulkanischen Aschen rezenter Eruptionen.

Schlüsselwörter: Pyroklasten, Reliktstrukturen, lithifizierte Tuffe, REM, sekundäre SEE-, Zr-, Y-führende Mineralien.

1. Introduction

"Many lithified volcaniclastic rocks are difficult to analyze microscopically because of the bewildering textural varieties resulting from the extensive dissolution of glass, the precipitation of diagenetic minerals and because of the small grain size of volcanic dust and some of the authigenic mineral phases" (FISHER & SCHMINCKE 1984: 313).

This quotation reflects the state of knowledge in the mid-eighties. Careful SEM studies, applying processed BSE imaging can give new insights into relict textures of shapes of shards and pumice fragments. Consequently, chemical composition, eruption and even deposition history can be reconstructed.

As a general definition of relict, we would like to refer to the American Heritage Dictionay. A geological relict is an adjective pertaining to something that has survived, such as structures or minerals after destructive processes. Pyroclast relict textures can be eruption-related. These are all textures deriving from pre- and post-depositional processes before the fragmented magma is thermally equilibrated with the environment. Hot water or steam, including vapor phase alteration can change the morphology of volcanic ash particles during the eruption. In accordance with primary structures, relict textures are a discriminating tool to reconstruct effusive and explosive eruptions (HEIKEN et al. 1989). Most pyroclast relict textures are mainly diagenesis-related. These are all textures deriving from post-depositional processes after the fragmented magma is thermally equilibrated with the environment. These include hydrothermal and lacustrine alteration, brines, groundwater alteration, alteration in the deep marine environment and burial diagenesis/metamorphism. The diagenesis-related textures should be considered in detail. There are three components which define an alteration environment: the composition of the starting material, physical conditions (temperature, grain size, porosity, permeability) and the composition of the pore solution (FISHER et al., 1984). Age, weathering and pressure by overburden can become additional parameters especially for older tuffs in the geologic record.

The selection of samples was mostly dominated by the first authors fieldwork studying the sedimentological features of the Triassic tuffs of the Southern Alps. Tuffs of various geological ages (Ordovician to Tertiary) had been studied as well. For most of them the pyroclastic origin was obvious, but except for chemical composition of the altered rock, nothing was known about fragmentation and deposition. Some of the pyroclastic rocks are totally overprinted by metamorphism and recystallization of metamorphic minerals. Others, as for example the Triassic tuffs from the Southern Alps (Italy) have almost intact pyroclast relict textures, although volcanic glass is totally absent. Tertiary bento-

nites from the Styrian basin (Austria) and for comparision the bentonites from the Mixteca Alta (Mexico) showed a variety of preserved relict textures and partially preserved glass. All examinations of the Styrian bentonites became a data base for the tephrachronology of the regional Miocene sediments (EBNER & OBENHOLZNER, in prep.).

One purpose of this study was to describe the dissolution of glassy volcanic ash particles and their replacement by secondary minerals related to post-depositional processes in which pyroclasts were thermally equilibrated with the environment. This paper can also be evaluated as a continuation of the studies of WISE et al. (1973). The textural evolution of pyroclastic rocks during burial diagenesis was also studied up to the reaction when analcime is converted to albite and water. The processes of hydration (water migrates into the glass) and devitrification (secondary crystallites are growing) of volcanic ash particles have been excluded, because they are described elsewhere (for references see FISHER & SCHMINCKE 1984: 312-340).

A second purpose of this study was to evaluate means by which eruption mechanism for altered pyroclastic rocks could be determined. Our main sources of comparison for this aspect were HEIKEN (1974) and HEIKEN & WOHLETZ (1985, 1996), who studied individual, three dimensional ash particles from historical eruptions. The results of those studies provide the basis of characterizing pyroclastic deposits from different eruption types. Shape analyses of pyroclast relict textures indicate for the studied non-welded and welded tuffs magmatic fragmentation of a primary silicic melt (see chapter 3: Case studies). The Triassic and Tertiary non-welded tuffs comprise a typical range of vesiculated and bubble wall shards (Y-shaped, curved, plate-like) and admixed pumice fragments, suggesting the eruption of highly vesiculated, heterogeneous melts. The preserved magmatic phenocrysts (biotite, feldspars, Fe-Ti oxides) and accessory minerals (zircon, allanite, apatite) support the reconstruction of chemical properties of these ancient magmas.

Many SEM-studied samples showed the same pyroclast relict textures that were seen with an optical microscope, but at a much higher resolution. We encountered several times, especially in altered welded tuffs, a discrepancy between the optical microscopic image and the digitized BSE image. Altered and devitrified welded tuffs often reveal under the optical microscope shard-like textures, which could not be detected on the BSE images; this discrepancy is mentioned in HEIKEN & WOHLETZ (1985). BSE images of these samples always show patchy intergrowths of quartz, K-feldspar, chlorite and/or illite, which do not mimic shard texture. We suggest that the optical microscope is able to detect mineral orientations or hydration fronts resembling shards, which cannot be seen on the BSE images.

All samples and SEM images (slides) of this project are available through the library of the Naturhistorisches Museum (NHM)/Mineralogie. Analyzed samples, localities and related images are listed as an appendix. Copies of sets of images, like pyroclast relict textures, magmatic, altered, secondary and REE-bearing minerals can be obtained for research or teaching purposes from the secretariat of the NHM/Mineralogie. A list of available sets can be provided and slides can be copied or photo CD-Roms are available at costs for reproduction and shipping. Please consult the homepage (http://www.nhm-wien.ac.at) of the Naturhistorisches Museum/Mineralogie for details.

2. Analytical procedure

2.1. Sample preparation

From all samples standard polished petrographic thin sections (20-30 µm thick) were prepared. In most cases the polishing of pre-existing petrographic thin sections provided excellent samples to work with.

Bentonite samples are slightly thicker and were polished with diamond powder (5, 3, 1 µm). For the final polish, dry Al203 (0.05 µm) was used. Imaging results showed that sample preparation did not destroy or dislocate even very thin layers (1 - 2 µm) of smectite in open vugs or vesicles. A variety of very pristine features like points of bubble wall shards and fibrous minerals (i.e. mordenite) growing in open pore space can be seen in thin or thick section. But to examine these minerals three dimensional samples should be preferred as the embedding in epoxy barely allows detailed shape analysis or the study of growth relationships.

Neither chemical nor ion beam etching of samples was necessary to perform as imaging clearly revealed shapes of pyroclastic particles. All samples were carbon coated using a LADD Vacuum Evaporator. Carbon coating allows average atomic number (Z) of minerals to control the intensity of BSE images. SEI was mostly utilized to see if minerals are on the surface of a thin section or if they are overlain by others.

2.2. Imaging techniques

Theoretical considerations about BSE imaging and applications for petrographic examination of sedimentary rocks can be found in many publications (see Further Reading). We used an ISI DS-130 Scanning Electron Microscope, equipped with a conventional analog imaging system, with a Robinson back scatter detector and Tracor Northern 5500 X-ray analyzer with Vista image processing, and a Noran Automated Digital Electron Microscope (ADEM) with integrated X-ray analysis and image processing (equivalent to a Noran 8500 system) at the EES-1, Geology & Geochemistry Facility of the Los Alamos National Laboratory.

A four step imaging at different magnifications of each sample allows an overview of particle size and/or preserved textures. At very low magnifications (ca. 20x) small scale sedimentary structures are apparent. Imaging at magnifications of ca. 50x, 150 - 200x and 400 - 500x provides the information for further investigations according to dominant particle size. Magnifications of 1000-10000x resolve intergrowth textures of matrix/cement phases.

The intergrowth of minerals of similar chemical composition (i.e. similar average atomic number), which may be hard to detect on a back scattered electron image, can be successfully documented by adjusting the image acquisition programs on both SEMs allowing image frames to be averaged pixel by pixel.

For standard investigations it was sufficient to average 20 - 30 image frames. Mineral associations, which show low contrast on the BSE image, can make it necessary to average 50 - 100 image frames. State-of-the-art SEMs have automatized image framing. Different

filtering functions provided by the image processing programs did not enhance particle shapes, but can create misleading artifacts. A detailed petrographic investigation of one sample, including sizing of particles, can easily take 8 - 10 hours.

Image processing programs on both SEMs provide sizing data according to the following parameters: area, perimeter, average diameter, length, width, shape factor (perimeter 2/(4 area)), aspect ratio (length/width) and orientation.

Usually it is difficult to relocate certain spots on a thin section, so we recommend careful analysis of the areas of interest before moving the sample stage. For the same reason all obtained images should be adequately photographed or stored, if the SEM is not equipped with a positioning system.

For image documentation we used the Rembrandt camera 3500F loaded with slide film. Slides can easily be organized in an archival form and are accessible at any time. Polaroid photos additionally document spots, where EDS analysis was performed. Digitized images can be stored on floppy discs for further image processing, especially sizing.

2.3. EDS analyses

Both SEMs were operated at 29 kV, at working distances of 18 - 25 mm and take-off angles of 40 degrees. EDS analysis should be performed according to standard operation procedures. For interpretation of EDS spectra the SEM Petrology Atlas by Joann & Welton (1984) is the most helpful publication. Another resource for EDS spectra of a variety of fumarolic minerals is the thesis of BERNARD (1985).

Many minerals occurring in altered pyroclastic rocks have similar chemical composition. In instances like these electron microprobe, transmission electron microscope or micro-XRD analysis is recommended. New results can be expected by application of ion microprobe or microscope and very high resolution field emission gun SEM analysis.

3. Case studies

3.1. Pyroclastic rocks altered to clay mineral-rich rocks: Miocene bentonites from the Mixteca Alta, SE Puebla, Mexico.

The Mixteca Alta contains widely scattered bentonite deposits, which recently have been explored by C. FABRY (Quimica Sumex, Puebla, Mexico). A preliminary SEM investigation was performed to prove the pyroclastic origin of these clay deposits. The shape of shards and pumice fragments or their relict textures are typical for non-welded, silicic tuffs. Sedimentary structures of these deposits are strongly obscured by the alteration process. The documentation of volcanic ash shards in bentonites was already done earlier by WISE et al. (1979, 1980) and KHOURY et al. (1979). Textural studies of bentonites had been performed by GRIM (1970), Ross (1928) and JEHN et al. (1974), mostly considering zeolites in bentonites.

Figure 1 is a low magnification overview showing glassy bubble wall shards (S1) side by side with shards replaced by smectite (S2), and totally (S3) or partially dissolved

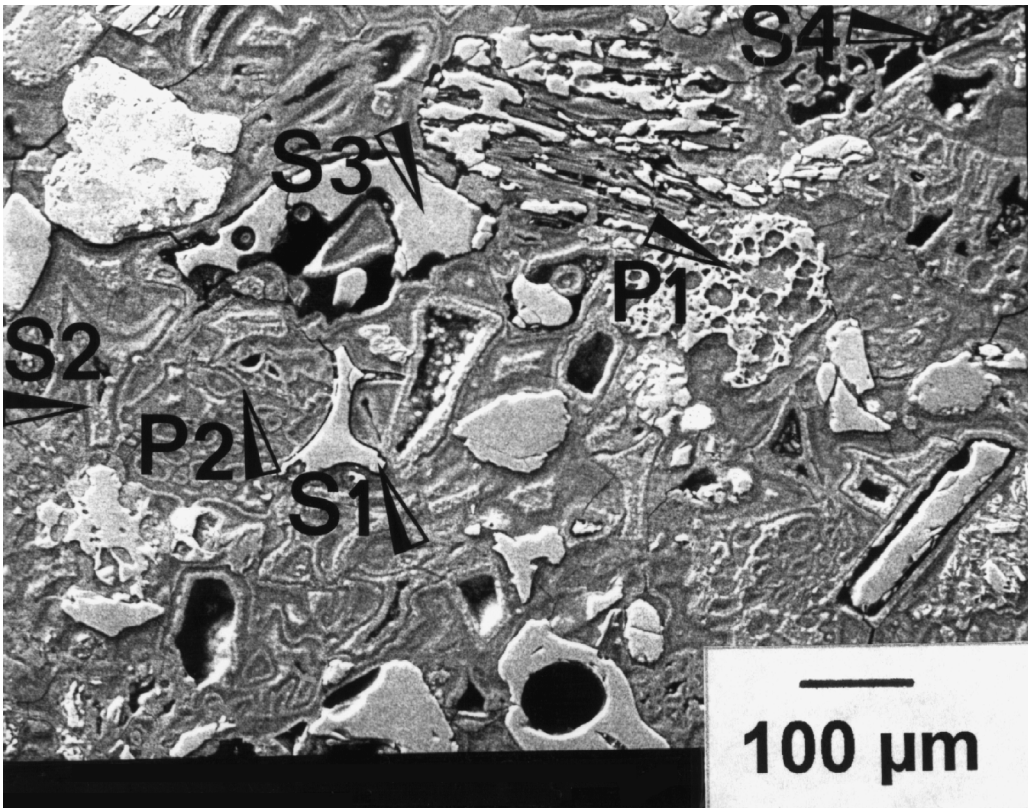

Fig. 1: Highly heterogeneous alteration conditions are standard for pyroclastic particles. Well preserved shards (S1) and pumice fragments (P1) occur beside dissolved or replaced shards (S2 - 4) and pumice fragments (P2). For further explanation see text. Locality El Rosario, Tertiary. BSE image.

glassy shards (S4), remaining as or surrounded by secondary pore space. The same can be observed for highly vesicular pumice fragments (P1, P2). Other fragments are broken feldspar crystals (grey) and altered Fe-Ti-oxides (white). All pyroclastic fragments and their replacement products are cemented by smectite. Two slightly different, chemical types of smectites can be recognized: a BSE-dark grey type outlining the shape relict of shard S2 and filling the central part of the interstitial space between particles; a BSE-light grey type filling the interior of the shape relict of shard S2 and forming coatings around particles.

Partially dissolved shard (S1) are characterized by many smooth, curved embayments, edges or pits (fig. 2). Empty pore space, resembling the original shape of the shard, remains. Early growth of smectites along the pyroclast edges and formation of interstitial cement can be seen. The central, nearly circular shaped cavities (C1) probably had been vesicles that became interconnected and enlarged throughout dissolution. Note that the remaining glass looks homogeneous on the BSE image, no hydration rims could be detected.

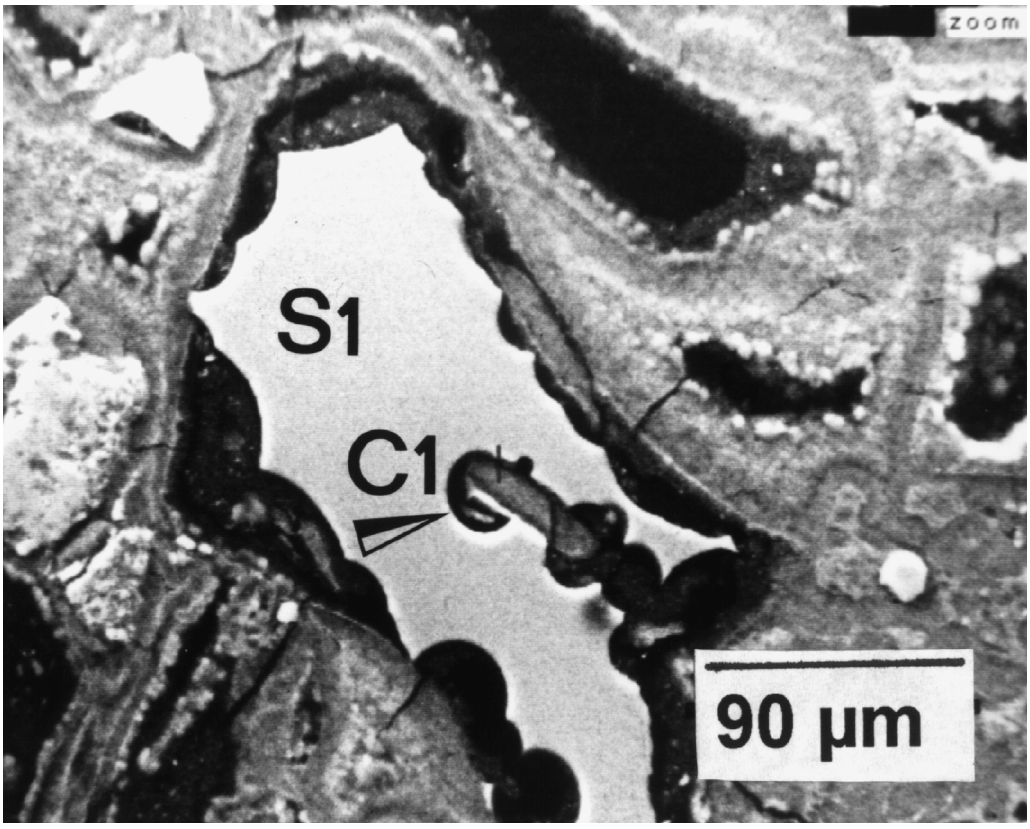

Fig. 2: Partially dissolved shard (S1) showing many smooth, curved embayments along the edges. For further explanation see text. Locality El Rosario, Tertiary. BSE image.

HEIKEN & WOHLETZ (1985) described SEM images of fractured surfaces of bentonite samples showing open cavities. These cavities resemble the shape of shards. The dissolved shard (S1) from figure 3 reveals a similar feature of empty pore space. The filling of former vesicles by smectite (SM1) and a late growth of another smectite population (SM2, light grey) along the inner edge of the pore space are bridging replaced vesicle space and former outer edges of the shard. V1 is a vug in the interstitial space between shard relicts, outlined by tiny silica spheres.

Figures 1 - 3 represent an alteration sequence observed within a set of samples collected at one site (locality El Rosario). Another bentonitized tuff is reported from the Mixteca Alta, which is, according to preliminary mapping, related to a different explosive event in the same area but similar in age and mineral content (locality Santa Maria Ayu). Even in totally bentonitized volcanic ash, where preserved magmatic minerals are rare, the pyroclast relict textures can be detected. Figure 4 shows the relict texture of a vesiculated shard replaced by smectite. Vesicle fillings and surrounding cement are smectite as well. The contrast on the BSE image between the interstitial cement, the replaced shard body and darker dots outlining the vesicles is caused by slight chemical differences in smectite

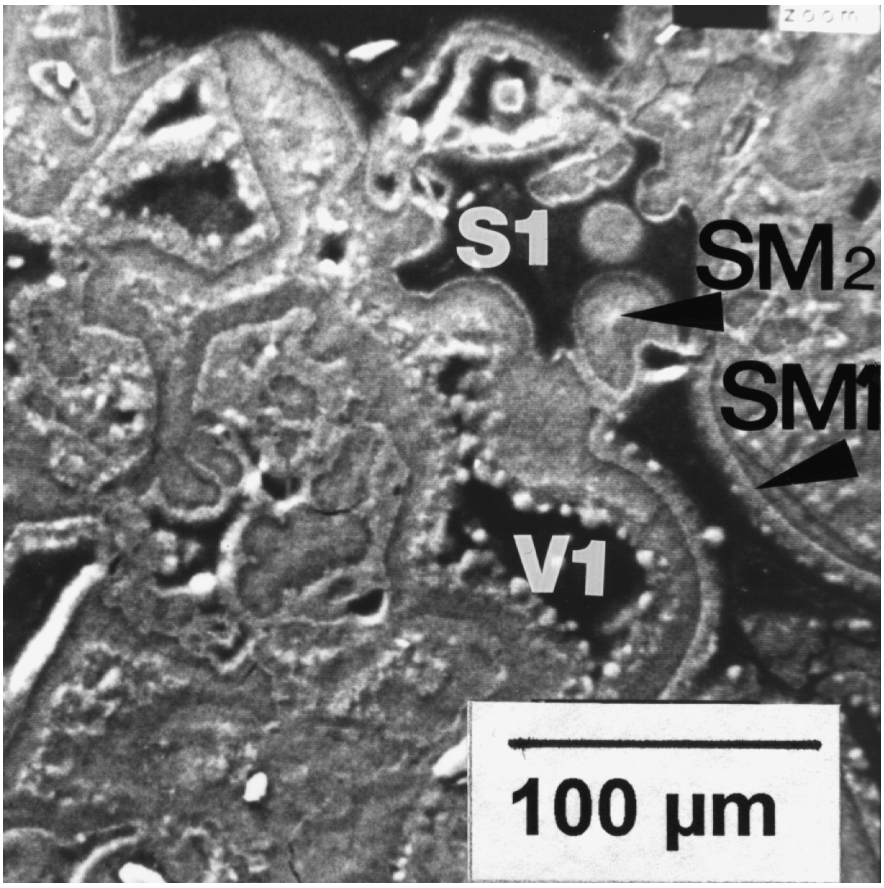

Fig. 3: Totally dissolved shard with vesicles replaced by smectite. Locality El Rosario, Tertiary. BSE image.

compositions. X-ray linescans indicate that for the shard-replacing smectite there are higher Al-, lower Si- and slightly higher Fe-contents than for the surrounding smectite.

At PHILIPS research laboratories a cathodoluminescence (CL) detector for electron microscopy was applied to these samples. CL contrast of chemically different clay minerals was not recognized, glass fragments of different degree of hydration showed detectable contrast in grey levels. Almost similar results could be obtained by OXFORD Instruments laboratories. Earlier CL studies of volcanic ash had been performed by DONAHUE (1969) for correlation purposes.

The bright white mineral inside one of the vesicles is barite, which is common in the studied Triassic and Tertiary altered tuffs. Trace element content and isotope ratios of authigenic barites could be used as a tool to characterize alteration environments and diagenetic processes (CHURCH 1979).

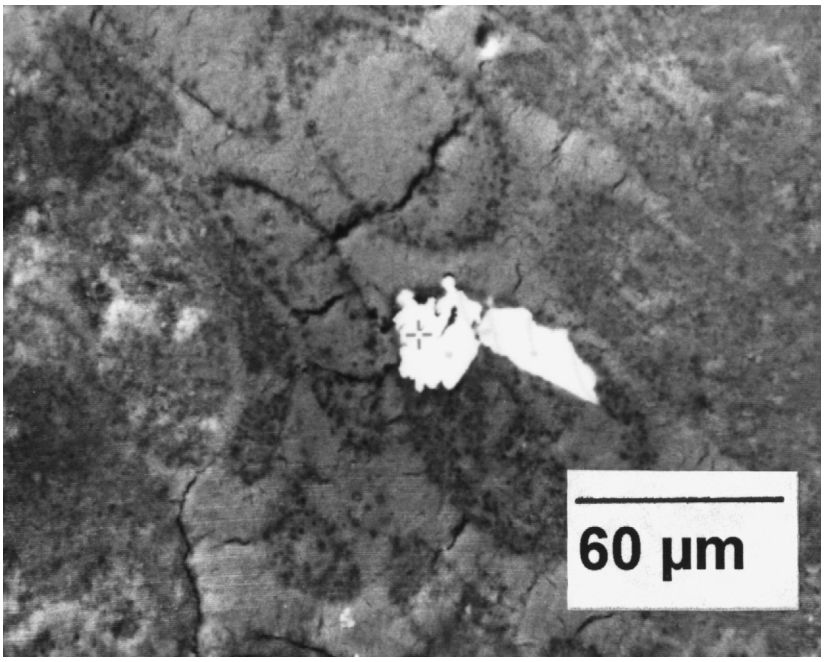

Fig. 4: Relict texture of a totally dissolved shard and vesicles, replaced by different smectites. The bright white mineral in the centre is barite. Locality Santa Maria Ayu, Tertiary. BSE image.

3.2. Pyroclastic rocks altered to chlorite-, analcime- or K-feldspar-rich rocks. Examples from the Triassic strata of the Southern Alps, Austria & Italy.

3.2.1. Relict texture of shards in non-welded tuffs

The products of Triassic volcanism are wide spread in the Southern Alps. For details see papers published by OBENHOLZNER (1991a) and OBENHOLZNER & HEIKEN (1999) and the literature quoted there. A first approach to an integration of these magmatic episodes into a more global model was published by VEEVERS et al. (1995).

Almost all of the known non-welded tuffs from the Triassic of the Southern Alps were deposited in a marine environment. Non-volcanic, sedimentary rocks at the base or at the top of volcaniclastic sequences are predominantly basinal or shallow marine limestones, and are used as an indicator for paleowater depth (OBENHOLZNER 1991a).

The Rio Fontanaz tuff is exposed in the Carnic Alps (N Italy), intercalated in a basinal marine succession. Shard shapes are very well preserved in the Rio Fontanaz Tuff. Figure 5 illustrates a topotaxitic relict texture of a vesiculated shard replaced by analcime (dark grey). Very thin vesicle walls are poorly preserved. The vesicles are filled with quartz (medium grey) and K-feldspar (light grey), showing various intergrowth textures. Dark grey patches inside the vesicles are analcime as well. Note the very smooth shape of the

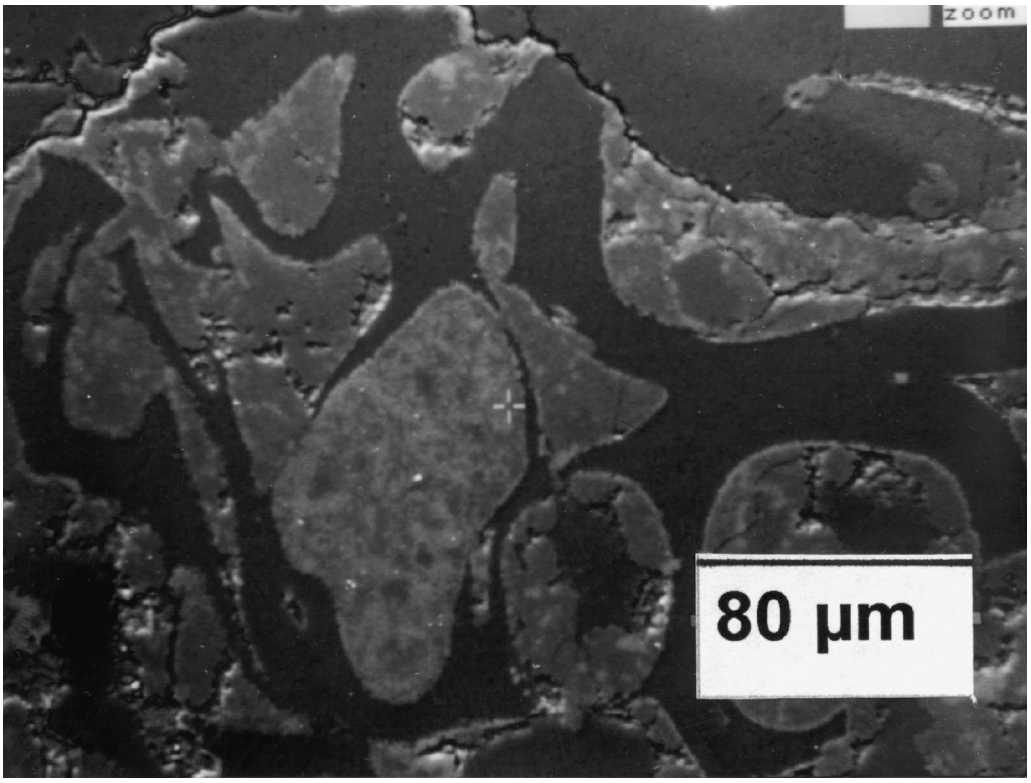

Fig. 5: Very well-preserved relict texture of a vesiculated shard replaced by analcime. Vesicle fillings are quartz, K-feldspar and analcime. Triassic. BSE image.

relict shard and the homogeneous replacement by analcime. Under the optical microscope relict shards can be detected, but the available resolution does not allow determination of the replacement mineral, mineral content of vesicle fillings or cement (OBENHOLZNER 1991a).

A very different style of topotaxitic replacement is documented by relict bubble wall shards from another Triassic tuff (Gartnerkofel tuff layer 2; Carnic Alps, Austria). This tuff layer was deposited on top of a shallow marine limestone. Fe-rich chlorite (white) replaces the main body of the shard and as a coarser crystalline variation it also fills the vesicles (figure 6). The shard edges and the vesicles are outlined by a K-Fe-bearing sheet silicate (KSS), which appears dark grey in the BSE image. The interstitial space between the relict shards is cemented by calcite (medium grey) and quartz (dark grey). The two phases might represent selective replacement conditions due to chemical differences between a probably hydrated rim and the main body of the shard. Under the optical microscope relict shards are recognizable, but appear to consist of homogeneous chlorite.

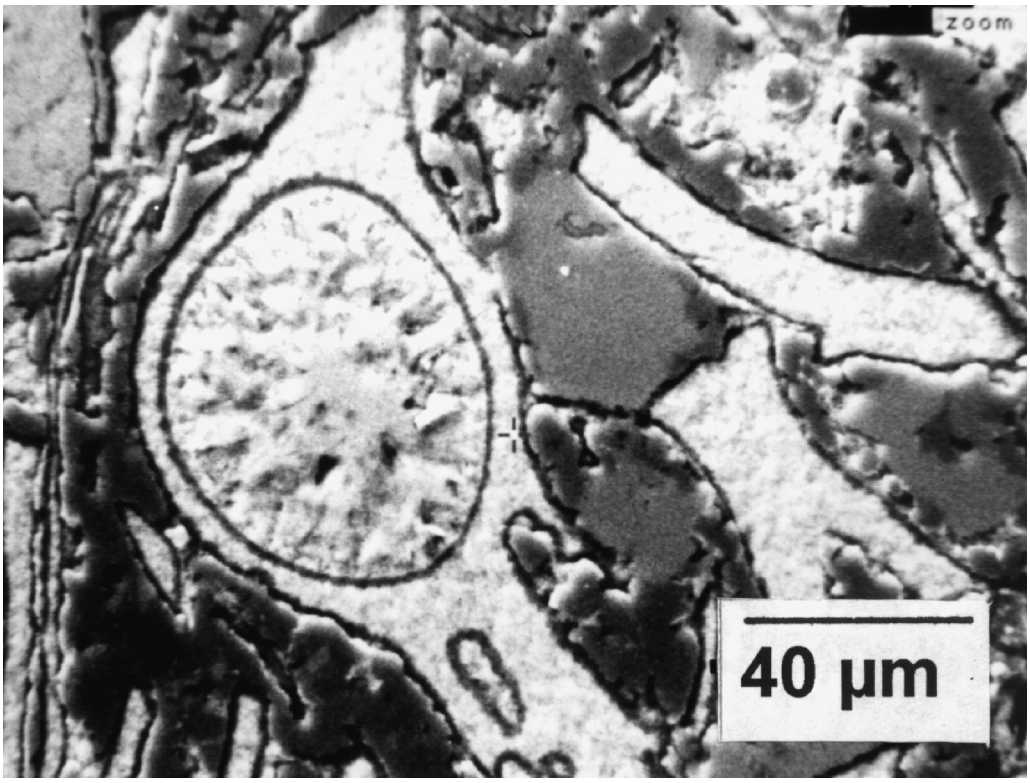

Fig. 6: Very well-preserved relict texture of bubble wall shards. Replacement minerals are Fe-rich chlorite and a KSS. For further discussion see text. Triassic. BSE image.

According to Federman (1984) silicic volcanic glass shards of Cenozoic age deposited in a deep marine environment do not show hydration rims, but hydration effects the entire shard. Commonly hydration rims are known from shards undergoing alteration in subaerial or shallow marine conditions. The setting and the replacement features of the Rio Fontanaz tuff and the Gartnerkofel tuff layer 2 fit very well within these observations. If these replacement features truly reflect depositional conditions and indicate paleoenvironments, they need further studies.

3.2.2. Relict texture of pumice fragments in non-welded tuffs

Pumiceous fragments are very common in the Rio Fontanaz tuff. They appear under the optical microscope as poorly differentiated chlorite patches. The BSE images reveal scattered quartz patches throughout a complex intergrowth texture of Fe-rich chlorite and KSS. The intergrowth textures may resemble textures of stretched and spherical vesicles (figure 7), but systematic studies demonstrated that very similar intergrowth textures of these two sheet silicates can be also obtained from non-replacing, diagenetic processes affecting glassy volcanic fragments in general. These intergrowth textures have been observed even as cavity or vug fillings.

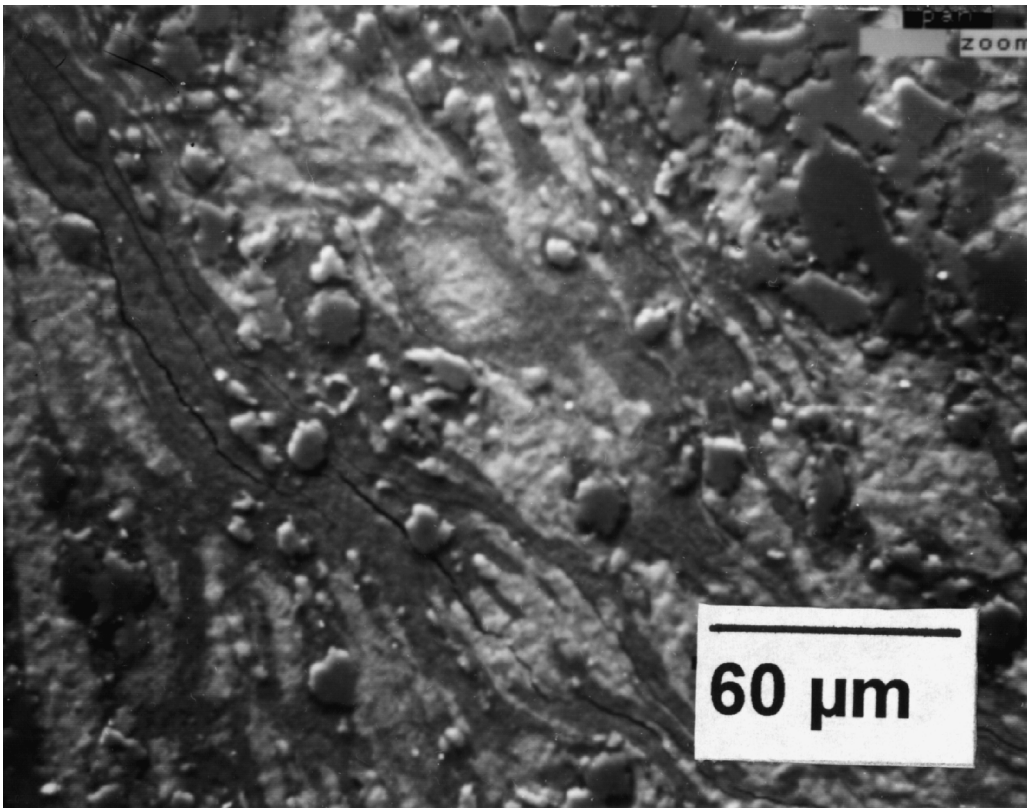

Fig. 7: BSE image of altered pumice. High-relief, grey minerals are quartz patches; low-relief, white mineral are Fe-rich chlorite; low-relief, grey minerals are KSS. Triassic Rio Fontanaz tuff. BSE image.

BSE images of the Gartnerkofel tuff layer 2 exhibit relict shards and mm-sized patches consisting of moss-like sheet silicates intergrowth and calcite (figure 8 & 9). Figure 9 shows the distinctively intergrown and irregularly distributed KSS (dark grey) and chlorite (white) patches. The first one could be attributed to the replacement of very thin vesicle walls of a pumice fragment, the latter one is considered to be a non-replacing, diagenetic product.

3.3. Pyroclast relict textures and diagenetic textures of welded tuffs

The interpretation of BSE images of altered welded tuffs remains contradictory. Optical microscopic images often show typical textures like flattened shards or collapsed pumice fragments (Ross & Smith 1961), whereas BSE images often reveal non-pyroclastic textures. This problem is documented by two case studies of Triassic welded tuffs from the Southern Alps.

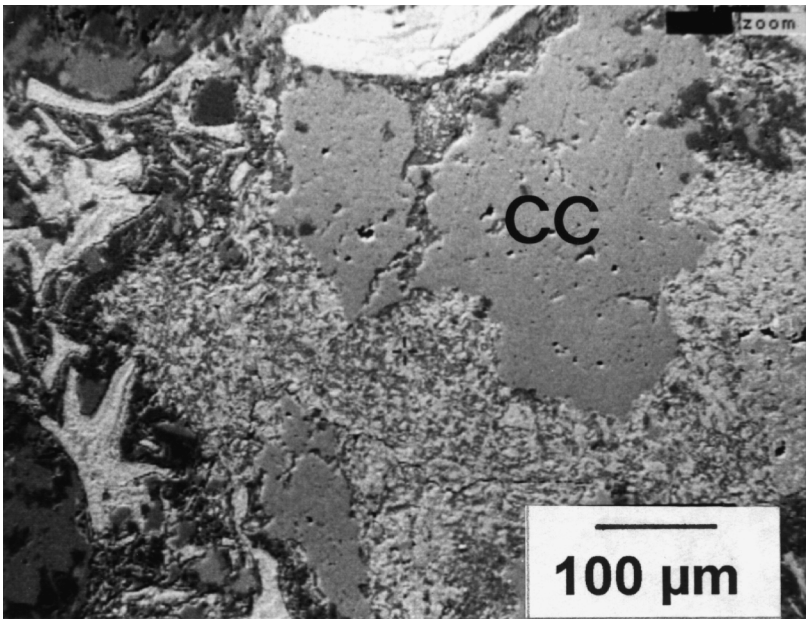

Fig. 8: Overview: chloritized shards (left) and highly altered pumiceous fragment showing moss-like intergrowth texture of Fe-rich chlorite and KSS, and partial, patchy replacement by calcite (Cc - medium grey). Triassic Gartnerkofel tuff layer 2. BSE image.

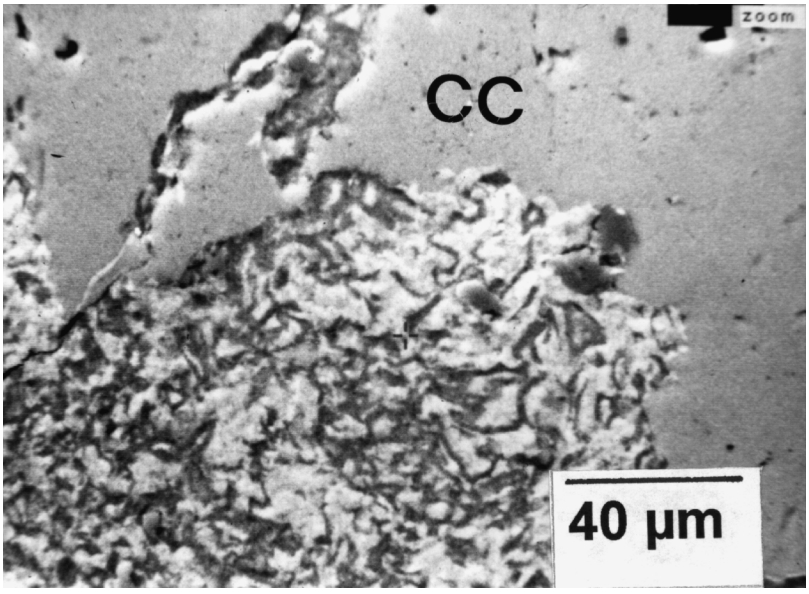

Fig. 9: Close-up of figure 8: the chlorite/KSS intergrowth does not clearly resemble vesicle filling in this pumiceous fragment. The grey mineral with smooth surface is calcite (Cc). Triassic Gartnerkofel tuff layer 2. BSE image.

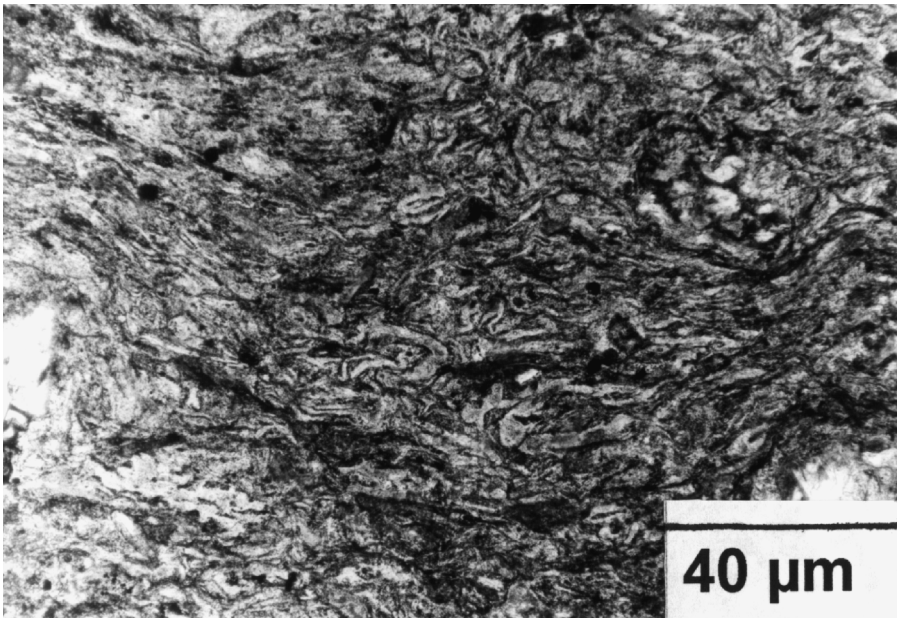

Fig. 10: Optical microscopic image of shard-like relict textures of the welded Gartnerkofel tuff 1. Triassic.

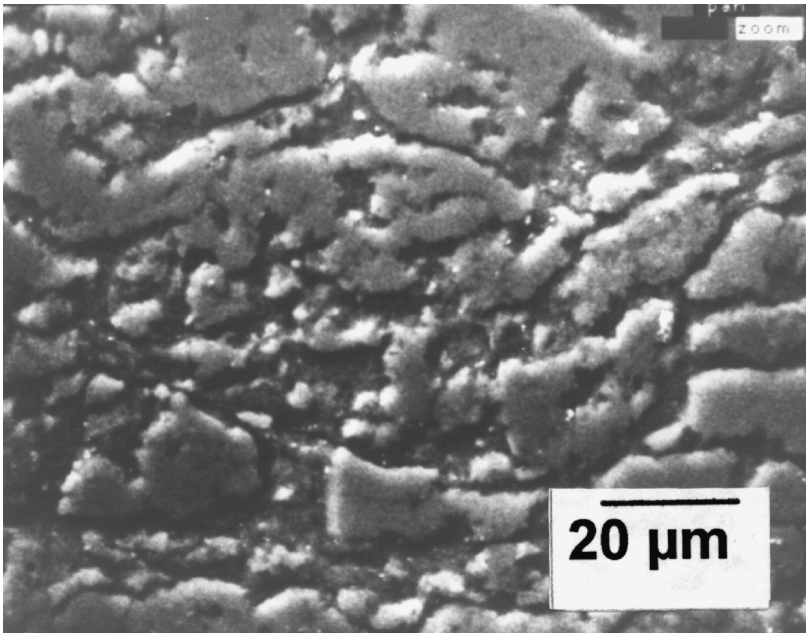

Fig. 11: BSE image of same sample as in figure 10. Patchy intergrowth of high-relief phases (quartz, K-feldspar) and low-relief phases (sheet silicates) without visible pyroclast relict texture. Triassic.

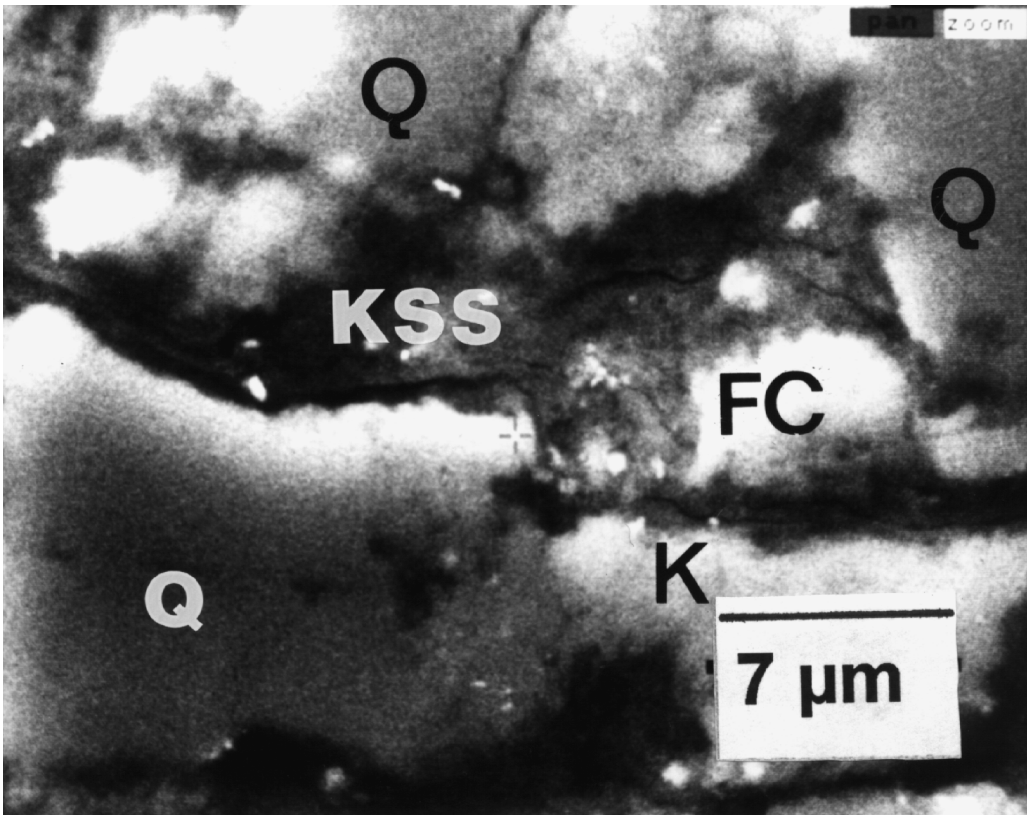

Fig. 12: Close-up of figure 11. High-relief, dark grey mineral is quartz (Q); high-relief, light grey mineral is K-feldspar (K); low-relief, white mineral is Fe-rich chlorite (FC); low-relief, dark grey mineral is KSS. Triassic. BSE image.

A well-documented example of this phenomenon is the dacitic Triassic Gartnerkofel tuff 1, a poorly to moderately welded tuff (OBENHOLZNER 1991b). Optical microscopic images show typical shard relict textures (fig. 10). BSE images from the same sample show instead of the expected enhancement of shard-like textures a patchy intergrowth of quartz, K-feldspar and chlorite/KSS (fig. 11 & 12).

The rhyolitic Triassic Rio Freddo ignimbrite (Julian Alps, N Italy) is a densely welded tuff (SPADEA 1970). Light microscopic images commonly reveal shard-like textures and collapsed pumice fragments. The most common texture found is an amoeboid, patchy intergrowth of K-feldspar (white) and quartz (dark grey) (fig.13 A). Quite rare relicts of shards (S1) can be observed, which are replaced by K-feldspar. Another rhyolitic Triassic welded tuff is exposed in the vicinity of Trzic (Slovenia). Collapsed pumices appear as ragged patches of micro crystalline K-feldspar without internal structure (figure 13 B) .

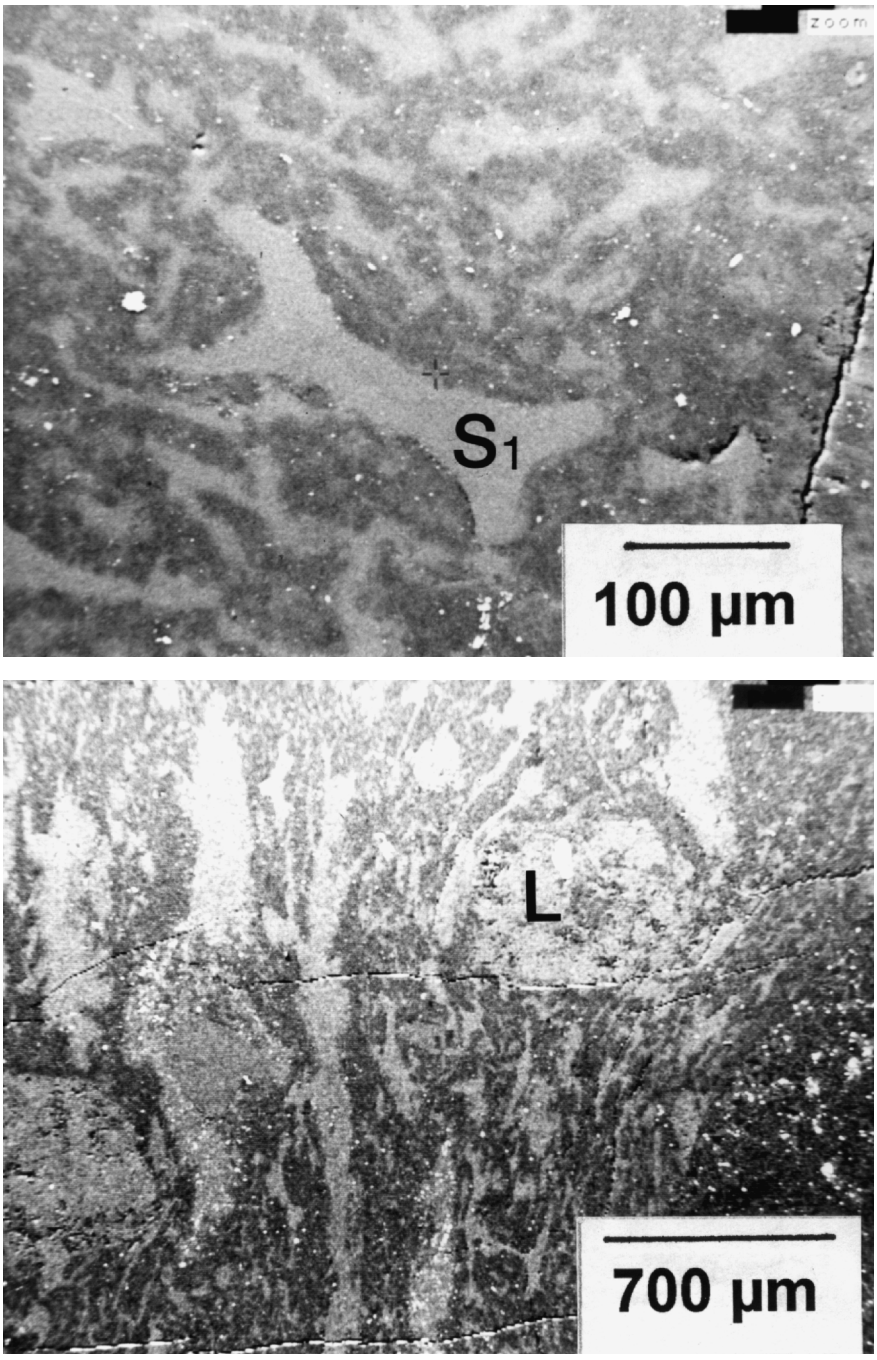

Fig. 13: (A) Rare relicts of shards (S1) occur in the quartz (dark grey) - K-feldspar (light grey) matrix of the Rio Freddo ignimbrite. Triassic. BSE image. (B) ragged patches of K-feldspar (light grey). Note that patches around lithics (L) are deformed - a typical compaction feature of welded tuffs. Triassic. BSE image.

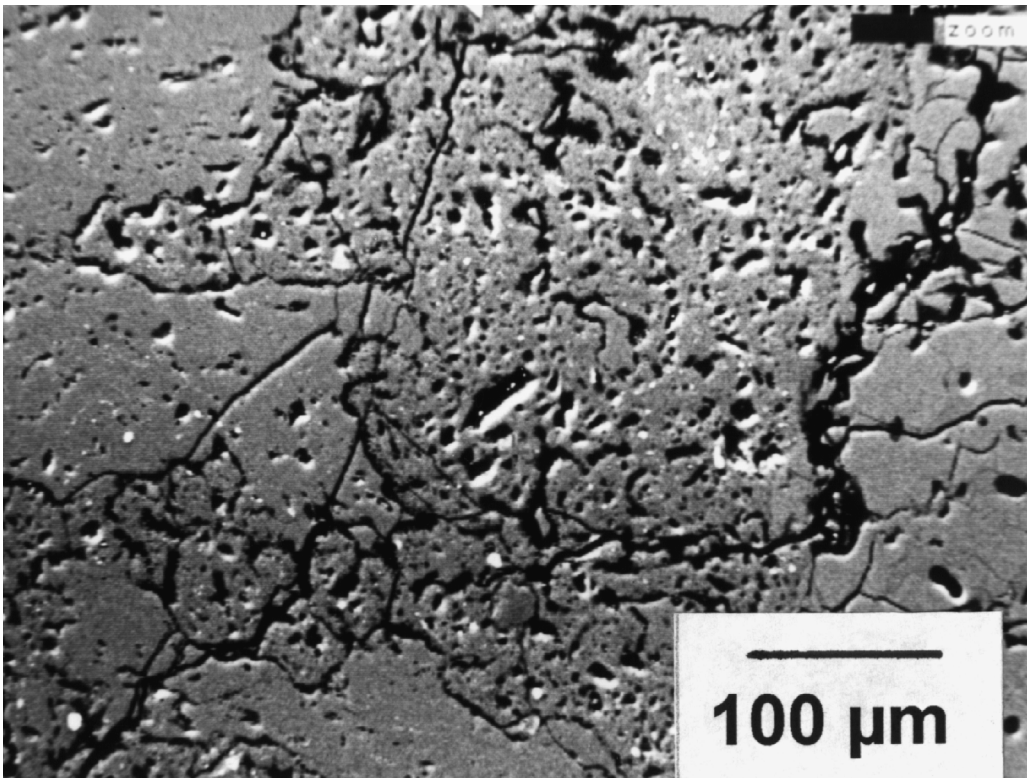

Fig. 14: Microporosity (black) of a young, densely welded tuff (Battleship Rock tuff, Valles caldera). Medium grey is glass showing no texture. Quaternary. BSE image.

Less altered, welded tuffs, like the Battleship Rock tuff (Valles caldera, New Mexico), reveal a microporosity (black) throughout the densely welded part (figure 14). Devitrification and the annealing of these amoeboid-shaped pores by secondary minerals could lead to matrix textures as observed in the Rio Freddo ignimbrite.

BSE images of altered welded tuffs also can enhance light microscopic images as reported by KOKELAAR & BUSBY-SPERA (1992) from the upper Triassic/lower Jurassic Vandever Mountain tuff (California).

4. Occurrence of secondary REE-bearing minerals in altered tuffs

Careful petrographical analysis utilizing the SEM demonstrated the occurrence of secondary REE-bearing minerals in altered tuffs of various ages. The very small size and the limits of EDS analysis prohibited identification of these minerals. State-of-the-art electron microprobe analysis (Cameca at LANL) was not successfull in identification although REE peak-overlap corrections can be handled to a certain degree (ROEDER 1985; BOTTAZZI et al. 1992). Preliminary electron microprobe studies suggest element ratios (wt.%) for secondary REE-carbonates: Ce:La:Nd:F:Ca = 7:4:3:1:4 and for secondary

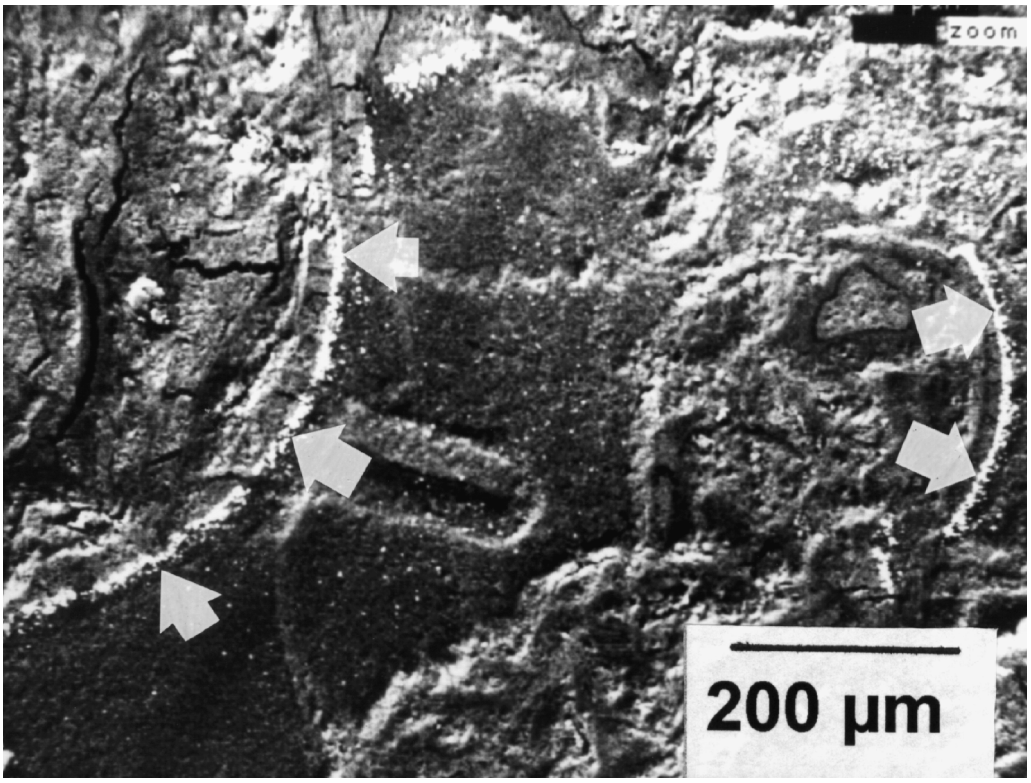

Fig. 15: Partially preserved relict texture of a bubble wall shard replaced by smectite. White arrows indicate distribution of unidentified La<Ce-mineral. Locality Santa Maria Ayu. Tertiary. BSE image.

REE-phosphates: Ce:La:Nd:P = 9:4:3:4. The electron beam also accelerates elements of the matrix minerals of the surrounding of the REE-bearing minerals. To our knowledge these occurrences are not mentioned in the scientific literature. Maybe related observations are published by BRUNO et al. (1989), MILODOWSKI et al. (1989), Rubin et al. (1989), HOLE et al. (1992), JANECKY et al. (1989) and DRISTAS et al. (1996). A preliminary presentation of two examples is given below to make other students of similar rocks aware of this phenomenon.

4.1. REE minerals outlining pyroclastic particles

Samples from the Miocene Mixteca Alta bentonites showed infrequently outlinings of partially preserved relict shards by a La<Ce-mineral (figure 15). The EDS diagram also shows small Y- and Th-peaks. The co-occurring Ca-, Al- and Si-peaks are probably generated by the smectite. The shard relict and the surrounding cement consist of smectite.

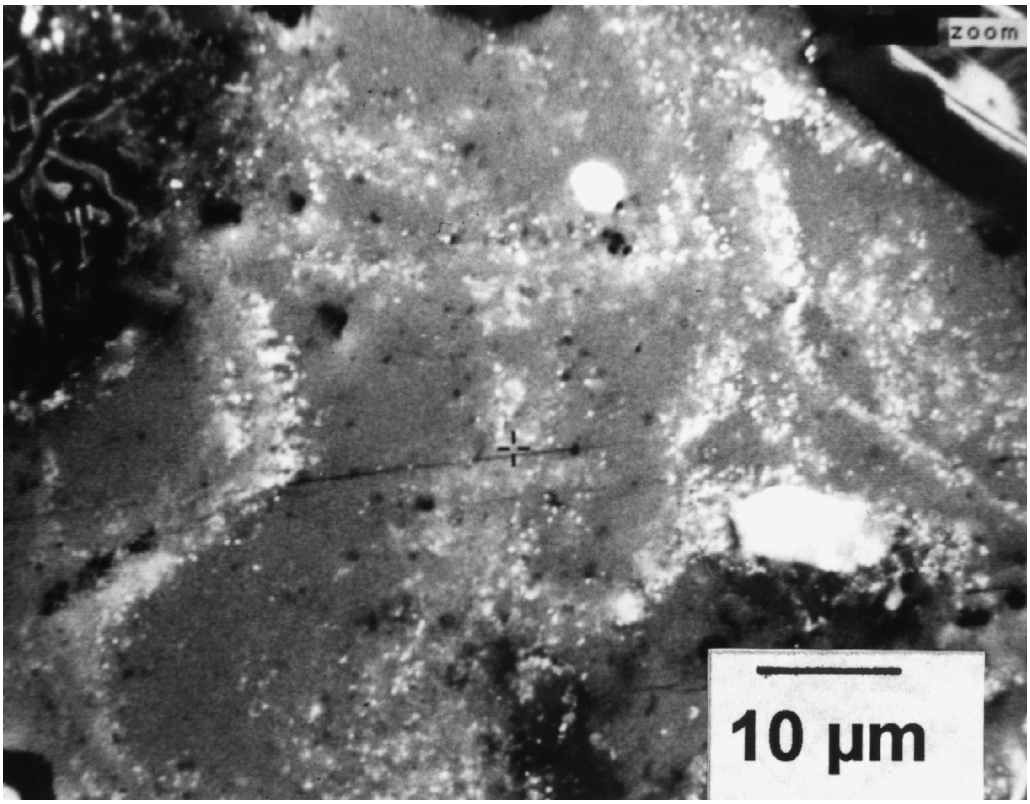

Fig. 16: Calcite filled vug in hydrothermally altered, welded tuff. Band-like oriented white dots are unidentified Zr>Y-Si-minerals. Triassic. BSE image.

4.2. REE minerals associated with hydrothermal textures

A hydrothermally altered part of the Rio Freddo ignimbrite contains vugs that are filled with calcite (medium grey), and a band-like oriented Zr>Y-Si-mineral (figure 16), which appears white on the BSE image. The white dots are smaller than 1 µm in diameter, so that only selected area EDS analyses could be performed. The larger white dot in the upper central part of the image shows an identical EDS pattern. Co-occurring Ca- and minor Mn- and Fe-peaks are generated by the surrounding calcite. The white mineral above the scale bar is apatite.

5. Acknowledgements

This project was sponsored by the Austrian Science Foundation (FWF) through an E. Schrödinger Grant to J.H. Obenholzner and by the Institute of Geophysics and Planetary Physics (IGPP) at the Los Alamos National Laboratory (LANL), under the auspices of the U.S. Department of Energy.

The authors are grateful to K. WOHLETZ (EES-1, LANL) for helpful discussion, C. LUCERO (D. Mann Petrographics, Ojo Caliente, New Mexico) for excellent sample preparation, C. FABRY (Quimica Sumex, Puebla, Mexico) for providing bentonite samples, R. RAYMOND and P. SNOW (both EES-1, LANL) for technical assistance at the SEM and helpful editing. G. KURAT (Naturhistorisches Museum/Mineralogie) provided helpful suggestions to finalize the manuscript.

References

BERNARD, A. (1985): Les Mechanism de Condensation des Gaz Volcaniques (Chimie, mineralogie et equilibres des phases condensees majeures et mineures). – These, Univ. Libre de Bruxelles, pp. 412.

BOTTAZZI, P., OTTOLINI, L. & VANUCCI, R. (1992): SIMS anayses of REE in natural minerals and glasses:an investigation of structural matrix effects on ion yields. – Scanning, **14**: 160-168.

BRUNO, J., CARROL, S., SANDINO, A., CHARLET, L., KARTHEIN, R. & WERSIN, P. (1989): Adsorption, precipitation and coprecipitation of trace metals on carbonate minerals at low temperature. – In: Miles, D.L. (ed.): Water-Rock Interaction (WRI-Six): 121-124.

CHURCH, T.M. (1979): Marine barites. – In: R.G. BURNS (ed.): Marine Minerals, Mineral. Soc. America, Short Course Notes, **6**: 175-209.

DONAHUE, J. (1969): Volcanic ash correlation by cathodoluminescence. – Geol. Soc. America Spec. Paper, **121**: 78.

DRISTAS, J.A. & FRISICALE, M.C. (1996): Lanthanoids enrichment in hydrothermally altered granodioritic rocks, Tandilia, Argentinia. – Terra Nostra, **8:** 37–38

FEDERMAN, A.N. (1984): Hydration of abyssal tephra glasses. – Jour. Non-Crystalline Solids, **67**: 323-332.

FISHER, R.V. & SCHMINCKE, H.-U. (1984): Pyroclastic Rocks. – Pp. 472. – Springer-Verlag.

GRIM, R.E. (1970): The texture and composition of bentonites. – Israel J. of Chemistry, **8**/3: 501-503.

HEIKEN, G. (1974): An Atlas of Volcanic Ash. – Smithsonian Contributions to the Earth Sciences, **12**: pp. 101.

—— & WOHLETZ, K. (1985): Volcanic Ash. – Pp. 246. – University California Press.

—— , SHERIDAN, M., WOHLETZ, K. & DUFFIELD, W. (1989): Textural distinction of silicic lavas and welded tuffs using processed scanning electron microscope images. – New Mexico Bureau of Mines & Miner. Res., **131**: 126.

HOLE, M.J., TREWIN, N.H. & STILL, J. (1992): Stability of the high field strength, rare earth elements and yttrium during late diagenesis. – Journal Geol. Soc. London, **149**: 689-692.

JANECKY, D.R., HAYMON, R.M., BENJAMIN, T.M., ROGERS, P.S.Z. & BAYHURST, G.K. (1989): Microscopic distribution of trace elements in minerals (chlorites, sulfides, sulfates) in submarine hydrothermal systems. – In: MILES, D.L. (ed.): Water-Rock Interaction (WRI-Six): 327-330.

JEHN, P.J., GUVEN, N. & BAILEY, J.F. (1974): Scanning electron microscopy of zeolites occurring in bentonites. – In: 32nd Annual Meeting, Electron Microscopy Society of America; Geology and Ceramics, Proceedings **32**: 458-459.

KHOURY, H.N. & EBERL, D.D. (1979): Bubble-wall shards altered to montmorillonite. – Clays and Clay Minerals, **27**/4: 291-292.

KOKELAAR, P. & BUSBY-SPERA, C. (1991): Subaqueous explosive eruption and welding of pyroclastic deposits. – Science, **257**: 196-201.

MILODOWSKI, A.E. & HURST, A., 1989. The authigenesis of phosphate minerals in some Norwegian hydrocarbon reservoirs: Evidence for the mobility and redistribution of rare earth elements (REE) and Th during sandstone diagenesis. – In: MILES, D.L. (ed.): Water Rock Interaction (WRI-Six): 491-494.

OBENHOLZNER, J.H. (1991a): Triassic volcanogenic sediments from the Southern Alps (Italy, Austria, Yugoslavia) – a contribution to the "Pietra verde" problem. – In: R. CAS & C. BUSBY-SPERA (Editors): Volcaniclastic Sedimentation. Sediment. Geol., **74**: 157-171.

—— (1991b): The Permian-Triassic of the Gartnerkofel-1 Core (Carnic Alps, Austria): Petrography and Geochemistry of an Anisian Ash-flow Tuff. – In: W.T. HOLSER & H.P. SCHÖNLAUB (Editors): The Permian-Triassic Boundary In The Carnic Alps Of Austria (Gartnerkofel Region). – Abh. Geol. Bundesanstalt, **45**: 37-51.

—— & HEIKEN, G. (1991): Relict shard textures – A comparison of a Triassic tuff with the 30 000 year old Campanian ignimbrite. – Abstract in IAVCEI proceedings, IUGG Vienna: p.15.

—— & HEIKEN, G. (1999): Relict Textures in the Rio Fontanaz Tuff- submarine or subaerial eruption of pyroclastic flows?– [Submitted to Acta Vulcanologica].

ROEDER, P.L. (1985): Electron-microprobe analysis of minerals for REE: use of calculated peak-overlap corrections. – Canadian Mineralogist, **23**: 263-271.

ROSS, C.L. (1928): Altered Paleozoic materials and their recognition. – AAPG Bulletin, **12/2**: 143-164.

ROSS, C.S. & SMITH, R.L. (1961): Ash-Flow Tuffs: Their Origin Geologic Relation and Identification. – Geol. Survey Prof. Paper, **366**: 81 pp. – Washington,

RUBIN, J.N., HENRY, C.D. & PRICE, G. J. (1989): Hydrothermal zircons and zircon overgrowths, Sierra Blanca Peaks, Texas. – Amer. Mineral., **74**: 865-869.

SPADEA, P. (1970): Le ignimbriti del membro superiore dalle Vulcaniti di Rio Freddo, nel Trias medio della regione di Tarvisio (Alpi Giulie Occidentali). – Studi Trentini di Scienze Naturali, Sez.A, Vol. **47/**N.2: 287-358.

VEEVERS, J.J. & TAWARI, R.C. (1995): Permian-Carboniferous and Permian-Triassic magmatism in the rift zone bordering the Tethyan margin of southern Pangea. – Geology, **23/**5: 467-470.

WELTON, J.E. (1984): SEM Petrology Atlas. – 237 pp. – Methods in Exploration Series. – Tulsa (AAPG).

WISE, S.W., WEAVER, F.M. & GUVEN, N. (1973): Early silica diagenesis in volcanic and sedimentary rocks: devitrification and replacement phenomena. – In: 31st annual meeting, Electron Microscopy Society of America: Proceedings (edited by C.L. Arceneaux), **31**: 206-207.

—— & WEAVER, F.M. (1979): Volcanic ash: examples of devitrification and early diagenesis. – Scanning Electron Microscopy, 511-518.

—— & AUSBURN, M.P. (1980): Kinney Bentonite: Re-Examined. – Scanning Electron Microscopy, 565-571.

APPENDIX

1. Further Reading on electron microscopy-related literature applied to geosciences:

BENNET, R.H., BRYANT, W.R. & HULBERT, M.H. (1991): Microstructure Of Fine-Grained Sediments. – Pp. 582. – Springer-Verlag.

BLOCK, A., VON BLOH, W., KLENKE, T. & SCHELLNHUBER, H.J. (1991): Multifractal analysis of the microdistribution of elements in sedimentary structures using images from scanning electron microscopy and energy dispersive x-ray spectrometry. – Jour. Geophys. Research, **96/**NO. B10: 16.223-16.230.

BUSEK, P.R. (Ed.): Minerals and reactions at the atomic scale: Transmission electron microscopy. – Reviews in Mineralogy, **27**: Pp. 508. – Mineralogical Society of America.

CHAPMAN, J.N. & CRAVEN, A.J. (1983): Quantitative Electron Microscopy. – Pp. 446.

CRAVEN, A.J. (1994): Electron Microscopy and Analysis 1993. – Pp. 546.

DAY, C. (1999): Electron cyromicroscopy comes of ages. – Physics today, March 1999: 21-22.

DINGLEY, D.J. & RANDLE, V. (1992): Review: Microstructure determination by electron backscatter diffraction. – Jour. Materials Sci., **27**: 4545-4566.

EXNER, H.E. & HOUGARDY, H.P. (1988): Quantitative Image Analysis of Microstructures. – Pp. 233. – DGM Informationsgesellschaft Verlag Oberursel.

FLEGLER, S.L., HECKMANN, J.W. & KLOMPARENS, K.L. (1993): Scanning and transmission electron microscopy. – Pp. 279. – Oxford.

GOLDSTEIN, J.I. & YAKOWITZ, H. (eds., 1975): Practical scanning electron microscopy: Electron and ion microprobe analysis. – Pp. 582. – New York.

—— , NEWBURY, J.I., ECHLIN, P., JOY, D.C., FIORI, C. & LIFSHIN, E. (1981): Scanning electron microscopy and X-ray microanalysis. A text for biologists, material scientists and geologists. – Pp. 673, New York.

GRABOWSKA, O.B. (1971): Examination of compacted sediments using the scanning electron microscope (translated title). Przeglad Geologiczne, **19**/8-9: 386-388. – Warsaw.

HEARLE, J.W.S., SPARROW, J.T. & CROSS, P.M. (1972): The use of the scanning electron microscope. – Pp. 278. – Oxford.

HILLIER, S. & CLAYTON, T. (1992): Cation exchange staining of clay minerals in thinsection for electron microscopy. – Clay Minerals, **27**: 379-384.

HOLT, D.B., MUIR, M.D., GRANT, P.R. & BOSWARVA, I.M. (1974): Quantitative scanning electron microscopy. – Pp. 570. – London.

HUMPHRIES, D.W. (1994): Methoden der Dünnschliffherstellung. – 86 pp. – Stuttgart (Enke).

KRINSLEY, D.H., PYE, K., BOGGS, J. & TOVEY, N.K. (1998): Backscattered Scanning Electron Microscopy and Image Analysis of Sediments and Sedimentary Rocks. – 193 Pp. – New York (Cambridge University Press).

LLOYD, G.E., SCHMIDT, N.-H., MAINPRICE, D. & PRIOR, D.J. (1991): Crystallographic textures. – Min. Mag., **55**: 331-345.

MARSHALL, J.R. (1987): Clastic Particles. Scanning Electron Microscopy and Shape Analysis of Sedimentary and Volcanic Clasts. – Pp. 346. – New York (Van Nostrand Reinhold Company).

MINNIS, M.M. (1984): An automatic point-counting method for mineralogical assessment. – AAPG Bulletin, **68**/6: 744-752.

NÖLTER, T. (1988): Submikroskopische Komponenten und Mikrotextur klastischer Sedimente. – Pp. 170. – Stuttgart (Enke Verlag).

PASTEK, M.T., HOWARD, K.S., JOHNSON, A.H. & MCMICHAEL, K.L. (1980): Scanning electron microscopy. A student's handbook. – Pp. 305.

PRIOR, D.J. & WHEELER, J. (in press): A study of an albite mylonite using electron backscatter diffraction. – Tectonophysics.

—— , TRIMBY, P.W., WEBER, U.D. & DINGLEY, D.J. (1996): Orientation contrast imaging of microstructures in rocks using forescatter detectors in the scanning electron microscope. – Min. Mag., **60**: 859-869.

PYE, K. & KRINSLEY, D. H. (1984): Petrographic examination of sedimentary rocks in the SEM using backscattered electron detectors. – Jour. Sed. Petrol., **54**/3: 877-888.

REIMER, L. (1967): Elektronenmikroskopische Untersuchungs- und Praeparationsmethoden. – Pp. 598. – Springer Verlag.

TRIMBY, P.W. & PRIOR, D.J. (in press). Microstructural imaging techniques: a comparison of light and scanning electron microscopy. – Tectonophysics.

VOGEL, W. (1994): Glass Chemistry. – Pp. 464. – Springer-Verlag.

WHITE, J.C. (ed., 1985): Short course in application of electron microscopy in the earth sciences. – Min. Ass. Canada. – Pp. 213. – Fredericton.

2. List of analyzed samples

Sample#	image#		image#		lithology, locality	age
DOB Xeno	3	14			Xenolith, Dobratsch, K,A	Triassic
RF4	17				Tuff, Rio Fontanaz, F, I	Triassic
FT4	18	79			Tuff, Rio Fontanaz, F, I	Triassic
O 3.5	80	87			Tuff, Rio Broite, F, I	Triassic
RB2B	88	90			Tuff, Rio Broite, F, I	Triassic
R203	91	116	184-200		Tuff, Rio Pecol Lungo,F,I	Triassic
2782 Trzic	117	127	129/150-183		welded tuff, Trzic, Sl	Triassic
97F88 Camp	130	149			Campanian Ignimbrite, I	Quartern.
54F88 Camp	201	208			Campanian Ignimbrite, I	Quartern.
96F88 Camp	209	232			Campanian Ignimbrite, I	Quartern.
W104B	233	256			Tuff, Drauzug, K, A	Triassic
9383 Gkofel	257	340			Tuff, Gartnerkofel, K, A	Triassic
FT12	341	-346	349/350/352	355/357	Tuff, Rio Fontanaz, F, I	Triassic
FT4	365	366A	368/371/2/374		Tuff, Rio Fontanz, F. I	Triassic
RB1=FT1.11	375	404			Tuff, Rio Broite, F, I	Triassic
Kerg RED	405	418-9	430	441	Ash, Kergeuelen Plateau	Quartern.
38945–NZ	442	448			Tuff, New Zealand	Permian
TI1	449				Tuff, Albania	Triassic
TI2	465				Tuff, Albania	Triassic
TI11	466				Tuff, Albania	Triassic
RPG/A Stmk.	467	516			Blasseneck-porphyroid, ignim.,A	Ordovician
RPG4 Stmk	517	617			Blasseneck-porphyroid, ignim., A	Ordovician
W105A	618	633			Tuff, Drauzug, K, A	Triassic
W39	634	666			Tuff, Drauzug, K, A	Triassic
W96	668	676			Tuff, Drauzug, K, A	Triassic
W102	677	691			Tuff, Drauzug, K,A	Triassic
W101	692	711			Tuff, Drauzug, K,A	Triassic
17971–Alb	712	736			Tuff, Albania	Triassic
4481	737	761			Karawanken, K, A	Triassic
OB19	762	786			Tuff, Karawanken, K, A	Triassic
T16 Dierico	787	836			Tuff, Dierico, F, I	Triassic
6387	837	861			Welded Tuff, Rio Freddo, F,I	Triassic
Z3Zelin	862	899			Tuff, Zelin, Sl	Triassic
B4Stmk	900	907			Bentonite, Stmk, A	Triassic
Dob8	908	966			Dobratsch, K, A	Triassic
B1Stmk	967	1005			Bentonite, Stmk, A	Triassic
MA21 Ung.Hu	1006	1013			Tuff, Hungary	Triassic
Sa1 Sauris	1014	1019			Tuff, Sauris, F, I	Triassic
PIC1 Koefels	1020	1037			"Pumice", Koefels, A	Quartern.
OT1 Oefenb.	1038	1045			Tuff, Oefenbach, S, A	Triassic
ITAlb.	1046	1058			Tuff, Albania	Triassic
W38	1059	1078			Tuff, Drauzug, K, A	Triassic

Sample#	image#		image#	lithology, locality	age
9885 Warch	1079	1085		Tuff, Drauzug, K, A	Triassic
286	1086	1140		Tuff, Kühweger Alm, K, A	Triassic
10085	1141	1173		Tuff, Gössling, K, A	Triassic
5787	1174	1202		Welded tuff, Rio Freddo, I	Triassic
8787	1203	1242		Welded tuff, Rio Freddo, I	Triassic
S14Alb	1243	1255		Tuff, Albania	Triassic
S38Alb	1256	1301		Tuff, Albania	Triassic
Ob19	1302	1340		Tuff, Karawanken, K, A	Triassic
2782	1341	1377		Welded tuff.,Trzic. Sl	Triassic
S14Alb	1378	1427		Tuff, Albania	Triassic
38945 NZ	1428	1433		Tuff, New Zealand	Triassic
BSR-wt	1440	1493		Welded tuff, Battle Ship Rock, NM, USA	Quartern.
587C	1494	1534		Welded tuff., Gartnerkofel, K, A	Triassic
Z12@	1535	1556		Tuff, Zelin, Sl	Triassic
Z12	1557	1575		Tuff, Zelin, Sl	Triassic
12080KW	1576	1593		Tuff, Karawanken, K, A	Triassic
RPL9	1594	1629		Tuff, Rio Pecol Lungo,F,I	Triassic
SA2–Sauris	1630	1652		Tuff, Sauris, F, I	Triassic
82729 Vetoe	1653	1671		Tuff, Hungary	Triassic
70816 Vetoe	1672	1684		Tuff, Hungary	Triassic
82732 Vetoe	1685	1700		Tuff, Hungary	Triassic
8383	1701	1742		Tuff, Möderndorfer Alm, K, A	Triassic
9383	1743	1764		Tuff, Möderndorfer Alm,A	Triassic
1182–Ob1	1765	1779		Tuff, Dobratsch, K, A	Triassic
R31C	1780	1855		Tuff, Rio Pecol Lungo, I	Triassic
R18	1856	1931		Tuff, Rio Pecol Lungo, I	Triassic
R8	1932	1941		Tuff, Rio Pecol Lungo, I	Triassic
Mex4	1942	1986		Bentonite, Mixteca Alta,Mx	Miocene
Mex5	1987	2007		Bentonite, Mixteca Alta, Mx	Miocene
Mex1	2008	2035		Bentonite, Mixteca Alta. Mx	Miocene
Mex3	2036	2080		Bentonite, Mixteca Alta, Mx	Miocene
ABL1/1	2081	2101		Bentonite, Mixteca Alta, Mx	Miocene
ABR1/1	2102	2119		Bentonite, Mixteca Alta, Mx	Miocene
Clay	2120	2134		Bentonite, Mixteca Alta, Mx	Miocene
Tu19B	2136	2147		Ash turbidite, RPL, F, I	Triassic
Tu2	2148	2164		Ash turbidite, RPL, F, I	Triassic
ARL1/2	2165	2191		Bentonite, Mixteca Alta, Mx	Miocene
ABR1/2	2193	2212		Bentonite, Mixteca Alta, Mx	Miocene
Shard Glen	2213	2224		Pottery , NM, USA	recent
RK1	2225	2226		Bentonite, Mixteca Alta, Mx	Miocene
Rch1	2227	2231		Bentonite, Mixteca Alta, Mx	Miocene
R30	2232	2240		Tuff, RPL, F, I	Triassic
Tu10	2241	2273		Ash turbidite, RPL, F, I	Triassic
Tu4	2274	2280		Ash turbidite, RPL, F, I	Triassic
Tu9	2281	2304		Ash turbidite, RPL, F, I	Triassic
Tu13	2305	2311		Ash turbidite, RPL, F, I	Triassic
Tu5	2312	2322		Ash turbidite, RPL, F, I	Triassic
Kerg RED	2323	2371		Ash, Kerguelen Plateau	Quartern.
TuYa	2372	2382		Ash turbidite, RPL, F, I	Triassic
62810 STMK	2383	2385		Bentonite, Stmk, A	Miocene
62821 STMK	2386	2389		Bentonite, Stmk, A	Miocene
62715 STMK	2390	2393		Bentonite, Stmk, A	Miocene
62799 STMK	2394	2397		Bentonite, Stmk, A	Miocene
62786 STMK	2398	2399		Bentonite, Stmk, A	Miocene
62791 STMK	2400			Bentonite, Stmk, A	Miocene

Sample#	image#		image#	lithology, locality	age
T4	2401	2404		Bentonite, Stmk, A	Miocene
62722 STMK	2405	2409		Bentonite, Stmk, A	Miocene
62724	2410	2413		Bentonite, Stmk, A	Miocene
StBart	2414	2415		Bentonite, Stmk, A	Miocene
62753 STMK	2416	2417		Bentonite, Stmk, A	Miocene
62712 STMK	2418	2420		Bentonite, Stmk, A	Miocene
62783 STMK	2421	2422		Bentonite, Stmk, A	Miocene
62731 STMK	2423	2425		Bentonite, Stmk, A	Miocene
62785 STMK	2426	2428		Bentonite, Stmk, A	Miocene
62743 STMK	2429	2430		Bentonite, Stmk, A	Miocene
Hochbruders	2431	2432		Bentonite, Stmk, A	Miocene
62741 STMK	2433	2434		Bentonite, Stmk, A	Miocene
62807 STMK	2435			Bentonite, Stmk, A	Miocene
62816 STMK	2436	2437		Bentonite, Stmk, A	Miocene
Buergerwald90	2438	2439		Bentonite, Stmk, A	Miocene
62852 STMK	2440			Bentonite, Stmk, A	Miocene
62751 STMK	2441			Bentonite, Stmk, A	Miocene
62772 STMK	2442			Bentonite, Stmk, A	Miocene
63603 STMK	2445	2447		Bentonite, Stmk, A	Miocene
62710 STMK	2443	2444		Bentonite, Stmk, A	Miocene
62716 STMK	2448			Bentonite, Stmk, A	Miocene
RuppB.Höhe	2449			Bentonite, Stmk, A	Miocene
62815 STMK	2450	2451		Bentonite, Stmk, A	Miocene
62770 STMK	2452	2491		Bentonite, Stmk, A	Miocene
62724 STMK	2492	2528		Bentonite, Stmk, A	Miocene
62743 STMK	2529	2542		Bentonite, Stmk, A	Miocene
62852 STMK	2543	2561		Bentonite, Stmk, A	Miocene
62807 STMK	2562	2584		Bentonite, Stmk, A	Miocene
62712 STMK	2585	2592		Bentonite, Stmk, A	Miocene
62816 STMK	2593	2613		Bentonite, Stmk, A	Miocene
62715 STMK	2614	2642		Bentonite, Stmk, A	Miocene
Buergerw.90	2643	2659		Bentonite, Stmk, A	Miocene
62751 STMK	2660			Bentonite, Stmk, A	Miocene
R134	2661	2677		Ash turbidite, RPL, F, I	Triassic
R79	2678	2688		Tuff, RPL, F, I	Triassic
R58	2689	2697		Tuff, RPL, F, I	Triassic
R40	2698	2701		Tuff, RPL, F, I	Triassic
MF1	2702	2741		Tuff, Monte Fioranca, F,I	Triassic
MF2	2742	2776		Tuff, Monte Fioranca, F,I	Triassic
MIAlb	2777	2791		Tuff, Albania	Triassic
119Alb	2792	2799		Tuff, Albania	Triassic
117aAlb	2800	2809		Tuff, Albania	Triassic
116ALB	2810	2815		Tuff, Albania	Triassic
116aAlb	2816	2823		Tuff, Albania	Triassic
114bAlb	2824	2835		Tuff, Albania	Triassic
Salb	2836	2840		Tuff, Albania	Triassic
U1	2841	2894		Tuff, RPL, F, I	Triassic
8787a	2895	2907		Tuff, Rio Salto, F, I	Triassic
287bGK	2908	2908		Tuff, Gartnerkofel, K, A	Triassic
5388	2919	2934		Welded tuff, Teufelsschlucht.,Sl	Triassic
2782	2935	2946		Welded tuff, Rio Freddo,F, I	Triassic
8483	2947	2970		Tuff, Möderndorfer .Alm, K, A	Triassic
118855CR	2971	2990		Tuff, Costa Rica	Quartern.
NYAO3	2991	3007		Tuff, Hungary	Tertiary
NYAo2B	3008	3024		Tuff, Hungary	Tertiary

Sample#	image#		image#	lithology, locality	age
KM1 ColMaar	3025	3052		Tuff, Colliseum Maar, Arizona, USA	Quartern.
MazO6	3053	3072		Tuff, Hungary	Cretac.
MazO7	3073	3093		Tuff, Hungary	Cretac.
MazO5b	3094	3107		Tuff, Hungary	Cretac.
MazO4	3108	3147		Tuff, Hungary	Cretac.
NYAO2bII	3148	3167		Tuff, Hungary	Cretac.
KA13	3168	3185		Tuff, Hungary	Tertiary
TT1	3186	3217		Tuff, Rio Broite, F, I	Triassic
TT3	3218	3245		Tuff, Rio Broite, F, I	Triassic
TT2	3550	3586		Tuff, Rio Broite, F, I	Triassic
SB191aObisp	3587	3612		Tuff, Obispo Fm, Ca, USA	Tertiary
Obispo fm	3400	3409		Tuff, Obispo Fm, Ca, USA	Tertiary
92982b Creede	3415	3438		Tuff, Creede Caldera, Co., USA	Quartern.
Maz5a	3439	3451		Tuff, Hungary	Cretac.
MP1Magdal	3613	3618		Bentonite, Mixteca Alta,MX	Miocene
MT1	3619	3623		Bentonite, Mixteca Alta,MX	Miocene
MT2	3624	3631		Bentonite, Mixteca Alta,MX	Miocene
AR1	3632	3634		Bentonite, Mixteca Alta,MX	Miocene
ROS40	3635	3637		Bentonite, Mixteca Alta,MX	Miocene
ROS41	3638	3641		Bentonite, Mixteca Alta,MX	Miocene
CT1	3642	3649		Bentonite, Mixteca Alta,MX	Miocene
I2	3650	3659		Bentonite, Mixteca Alta,MX	Miocene
HU1	3660	3669		Bentonite, Mixteca Alta,MX	Miocene
AB1	3670	3678		Bentonite, Mixteca Alta,MX	Miocene
ROS42	3679	3686		Bentonite, Mixteca Alta,MX	Miocene
ROS43	3687	3698		Bentonite, Mixteca Alta,MX	Miocene
AB2	3699	3704		Bentonite, Mixteca Alta,MX	Miocene
MP1	3705	3712		Bentonite, Mixteca Alta,MX	Miocene
MP2	3713	3723		Bentonite, Mixteca Alta,MX	Miocene
Ob97SelXen	3724	3740		Xenolith, Seleniza, K, A	Triassic
Ob619382Gri	3741	3745		Lava, Karawanken, K, A	Triassic
315824Yucc	3746	3460		Tuff, Yucca Mts., Nevada, USA	Tertiary
Shard–Glen	3761	3772		Pottery, NM, USA	recent
10483 moed	3773	3789		Tuff, Karnische Alpem, K, A	Triassic
8083	3790	3796		Tuff, Möderndorfer Alm, A	Triassic
50283	3797	3807		Tuff, Möderndorfer Alm, A	Triassic
NYAo1	3808	3809		Tuff, Hungary	Tertiary
NYA2a	3810	3824		Tuff, Hungary	Tertiary
287Ctem	3825	3846		Tuff, Gartnerkofel, K, A	Triassic
92982G	3847	3854		Tuff, Creede Caldera, Co., USA	Quartern.
82743 hun	3855	3858		Tuff, Hungary	Triassic
82731 hun	3859	3865		Tuff, Hungary	Triassic
82730 hun	3866	3872		Tuff, Hungary	Triassic
82728 hun	3873	3881		Tuff, Hungary	Triassic
8787a	3882	3889		Tuff, Rio Salto, F,I	Triassic

Abbreviations: Cretac. = Cretaceous; Quartern. = Quarternary; A = Austria, K = Kärnten (Carinthia), Stmk/STMK = Steiermark (Styria), S = Salzburg County; I = Italy, F = Friuli, RPL = Rio Pecol Lungo; Ung/Hu = Hungary; SL = Slovenia; MX = Mexico; USA: Ca = California, Co = Colorado, NM = New Mexico.

Comments: The Triassic tuffs are subaqueously deposited, mostly pyroclastic flow deposits and ash fall deposits (i.e. Drauzug tuffs). The depositional environment of Triassic welded tuffs remains problematical, they are mostly intercalated between marine sediments.